

# ULTRA-BROADBAND INTEGRATED INTERFEROMETRIC OPTICAL MODULATORS

Le N. Binh and Thiam W. Chua

Laboratory for Optical Communications and Applied Photonics, Department of Electrical and Computer Systems Engineering, Monash University, P.O. Box 35, Clayton, Victoria 3800, Australia

Email: le.nguyen.binh@eng.monash.edu.au

## SUMMARY

*Integrated optical modulators operating at multi-GHz region are critical for Tera-bps optical communications systems and networks. This paper describes a simple, efficient and accurate analysis of the travelling wave electrodes for high-speed optical modulation and the implementation of these electrodes in interferometric optical modulators for broadband operation in the microwave and mm-wave region. Such integrated optic modulators are formed with an interferometric optical waveguide structures in which one arm of the interferometer is phase modulated with a travelling electrical electrode.*

*A finite difference approach is used for modelling the travelling wave electrodes for efficient electro-optic interaction in interferometric optical modulators. UV lithographically fabricated electrode configurations such as symmetric and asymmetric co-planar waveguide or strip structures can be modelled. Simulated results demonstrate the efficiency of the presented method are compared with ones obtained by other methods such as the Green's function, conformal mapping, method of images, spectral domain analysis etc.*

*Tilted and thick practical electro-plated electrodes are modelled and confirmed with implemented modulators operating up to 26 GHz in diffused LiNbO<sub>3</sub> optical interferometric optical waveguide structures. The fabrication of optical waveguides and travelling wave electrodes are described for implementation of the electro-optic interferometric modulators.*

## 1 INTRODUCTION

Optical communication systems have now reached an increasing fast pace in both speed and capacity with 10 Gb/s OC-192 then 40 Gb/s OC-768 and beyond, e.g. optical transmitters for 80 Gbps and 160 Gbps in the near future. External modulation is the only possible technique for modulation of lightwaves at bit rate greater than 10 Gbps. Electrooptic modulators in LiNbO<sub>3</sub> guided-wave structures have been contributing significantly in the last two decades in the technological evolution of optical fibre communications due to its intrinsic high-speed property. Furthermore in order to avoid the optical nonlinearity in wavelength multiplexed optical transmission in optical fibres, it is necessary that the total average optical power is reduced below the nonlinear threshold, about 5 dBm for standard single mode optical power. One probable technique is to suppress the optical carriers i.e. generating modulated lightwaves of 180° phase shift in the two arms of the interferometer. This modulation format of carrier-suppressed return-to-zero (CS-RZ) requires two interferometric modulators in tandem. This demands an efficient and accurate modelling of the travelling wave electrodes and the interaction of the launched travelling waves in such combined electro-optic modulation system.

This paper thus presents a simple but very efficient model for the design of interferometric optical modulators in which travelling wave electrodes are integrated with optical interferometric waveguide structures. That is an implementation of a dynamic Mach-Zhender interferometer (MZI) using integrated optic technology. The implementation of such modulators in LiNbO<sub>3</sub> substrate is also briefly described. Our model proves to be very efficient for practical implementation of a broadband MZI modulator operating up to 26 GHz, particularly when the electrode structures do not follow an ideal brick-wall like feature.

The design of travelling wave electrodes is established based on an empirical model that is derived from the combination of the quasi-TEM analysis and the Green function method. This model primarily allows a simple evaluation of the structure of the electrode. It does not generate the transverse electric fields that are mandatory for calculations of the overlap integral between the guided optical fields and the electric field of the microwave travelling waves. More importantly, it does not take into account of the more subtle structural factors such as the wall angle of the gold plated electrode<sup>[21]</sup>. Most analyses such as the conformal mapping technique<sup>[1]</sup>, the Green function method<sup>[4-5]</sup> or the method of images<sup>[3,15]</sup>, either assumes an infinitely thin electrodes and 90° wall angle of the electrode.

When very thick electro-plated electrodes, typically in the range of 10 to 20 μm<sup>[20,21]</sup>, are fabricated to increase its impedance and hence broadband matching, with a bandwidth of more than 40 GHz, the assumption of 90° brick-wall like angle is no longer accurate. In practical devices, after the electro-plating process, the electrode normally assumes a trapezoidal shape as shown in Figure 1(b). Figure 1(a) shows the schematic plane view of the electro-optic interferometric optical modulators. The wall angle of the electrode has a significant influence on the effective microwave index  $n_m$  and its characteristic impedance  $Z$ . It is therefore important to take into considerations such structural effects of the electrodes in the design of the travelling wave electrodes.

Chung et al.<sup>[4,5]</sup> modelled the electric field of the electrodes with the Green function method. Unfortunately the effect of the wall angle has not been taken into account. Such electrode structural factors can only be modelled by a more robust numerical formulation such as the finite element method<sup>[12-13, 18, 19-20]</sup>. The finite difference method developed in this work is unique for solving the anisotropic Laplace equation due to its relative simplicity and sufficiently accuracy and consistent with the experimental results.

This paper is organised as follows. In the next section we outline the numerical formulation using the finite difference with non-uniform grid mesh for solving the anisotropic Laplace equation under the assumption of quasi-TEM of the microwave travelling mode. Based on this numerical model, the analytical system, the Finite Difference Travelling Wave Electrodes Analysis (FDTWEA), is developed to model the electrode parameters  $Z$  and the microwave effective index  $n_m$ . The transverse optical modulated fields,  $E_x$  and  $E_y$ , and the interaction overlap efficiency between the travelling microwave and these guided optical waves, of broadband interferometric optical modulators are then described. Comparisons of our calculations with published results to verify the validity, the simplicity and the efficiency of FDTWEA are then given.

The effects of the tilted angle of the electroplated wall of the electrode are investigated. Analysed electrodes are designed and optimised taking into considerations of the interferometric optical waveguides for maximising the operating bandwidth of optical modulators. The implementation of the interferometric modulators operating up to 30 GHz is briefly described in Section 3. Finally concluding remarks on the developed model and the fabricated MZI modulators are given.

## 2 ELECTRODE MODELS AND ELECTRO-OPTIC INTERFEROMETRIC MODULATION

### 2.1 A Finite difference model for RF travelling wave electrodes

Travelling wave electrodes in integrated optical modulators are miniaturised transmission lines where quasi-TEM wave propagation can be assumed. The electric field can then be approximated by a two-dimensional electrostatic field problem that can be modelled by Laplace equation. Z-cut LiNbO<sub>3</sub> crystal substrate is employed due to its large electro-optic coefficient. Other substrate orientations X- or Y-cuts can be adapted without any difficulty by taking into account appropriate tensor properties of the electro-optic interaction. The permittivity tensor matrix takes a diagonal form<sup>[1]</sup> and the electrostatic potential  $V$  is essentially the solution of the anisotropic Laplace equation given by

$$\frac{\partial}{\partial x} \left( \epsilon_x \frac{\partial V}{\partial x} \right) + \frac{\partial}{\partial y} \left( \epsilon_y \frac{\partial V}{\partial y} \right) = 0 \quad (1)$$

The device under consideration is discretised into a grid plane. Either uniform or non-uniform meshes can be used to economise the computing computer memory. Denser meshes are allocated at the edges of the electrode and also the buffer layer area so that the effect of the edge of the electrode on the electric fields can be more accurately estimated. On the other hand nodes located further away from the electrode can be modelled with a coarser mesh.

The steps involved in formulating the difference equation<sup>[19]</sup> are described in the followings. Considering a general electrode structure as shown in Figure 2 with grid points placed along dielectric boundary, the electrode structures involve only three dielectric media, namely, the air region, the SiO<sub>2</sub> layer and the LiNbO<sub>3</sub> substrate. Boundary conditions can be considered for nodes positioned along the boundary, say P and four other points surrounding it, namely, A, B, C and D. The difference relationships of the mid-points between AP, BP, CP and DP labelled in order of 1, 2, 3 and 4 and their respective grid sizes are denoted as  $h_a$ ,  $h_b$ ,  $h_c$  and  $h_d$  can be established. Their corresponding electrical field potentials can then be obtained.  $V_P, V_A, V_B, V_C$  and  $V_D$ , respectively.  $K_{e1}$  and  $K_{e2}$  are the dielectric constants of the medium via the discretised Laplace equation (1) as

$$\frac{\left( \epsilon_x \frac{\partial V}{\partial x} \right)_{PB} - \left( \epsilon_x \frac{\partial V}{\partial x} \right)_{AP}}{\frac{1}{2}(h_a + h_b)} + \frac{\left( \epsilon_y \frac{\partial V}{\partial y} \right)_{PC} - \left( \epsilon_y \frac{\partial V}{\partial y} \right)_{DP}}{\frac{1}{2}(h_c + h_d)} = 0 \quad (2)$$

A five-point difference relationship can be obtained for inner elements and for boundary elements can be formulated as illustrated in Figures 1 and 2 at the interface between air and the SiO<sub>2</sub> buffer layer and that for the buffer layer and the substrate. Furthermore for nodes located inside the electrode region a zero electric field conditions are applied. Using a sufficiently large space of approximately  $400 \times 400 \mu\text{m}$ , the electric field along the boundaries are assumed to be negligible. For the field potential, it is essential that Neumann boundary conditions<sup>[19, 30]</sup> should be established. The rest of the windows are just the permutation of the boundary conditions. Incorporating the boundary conditions into the difference equations, a set of difference equations can be derived from each grid point resulting in an eigen-matrix equation

$$\mathbf{A}\cdot\mathbf{u}=\mathbf{b} \quad (3)$$

where  $\mathbf{A}$  is the coefficient matrix,  $\mathbf{u}$  is the vector representing the potential at grid points, while  $\mathbf{b}$  is the vector that assumes the RHS of (1) whose elements take many zeroes except where corresponding to those of the grid points positioned on the electrodes. Figure 2(a) shows the grid size and the formation of the matrix coefficients.

The difference matrix equation can be solved by conventional successive over the relaxation method<sup>[19,30]</sup> which requires a good initial guess and an appropriate estimate of the relaxation factor in order to obtain a reasonable rate of convergence. Using ITPACK NSPCG<sup>[31]</sup>, the eigenvalue matrix can be solved relatively quickly with high accuracy. ITPACK matrix solver applies various accelerators and preconditioners in solving the matrix. For banded matrices, only the nonzero elements are stored so as to significantly economise the computer memory. The Othormin accelerator and incomplete Cholesky preconditioner can be used<sup>[31]</sup> and the solution of the anisotropic Laplace equation enable calculations of various properties of the microwave electrodes.

## 2.2 Line capacitance, characteristic impedance and microwave effective index of the travelling microwaves

The main parameters of the microwave electrodes, the characteristic impedance  $Z$  and the microwave effective index  $n_m$  can be determined by

$$Z = \frac{1}{c\sqrt{CC_0}} \quad (4)$$

$$n_m = \sqrt{\frac{C_0}{C}} \quad (5)$$

where  $C$  is the capacitance per unit length of the transmission line in the dielectric substrate, while  $C_0$  is the capacitance per unit length for the air filled medium, with  $c$  speed of light in vacuum. To obtain the capacitances, the charges on the conductors are calculated by the Gauss's theorem<sup>[26]</sup>. The integration of the normal component of the electric flux is conducted over a surface enclosing the 'hot' electrode as shown in Figure 2(c). Forming this surface by lines joining the nodal points drawn parallel to the coordinate directions at any point  $P$  on this surface, we have

$$D_n = \varepsilon E_n = -\varepsilon \frac{\partial \mathcal{V}}{\partial n} \quad (6)$$

where  $D_n$  is the normal component of the electric flux,  $E_n$  is the normal component of electric intensity, and  $n$  is the normal coordinate, which for a square box would be  $x$ , and  $y$ . The potential at  $P$  may be expressed in terms of the known potentials  $V_A$  and  $V_B$  on each side of it. For irregular mesh shown in Figure 2(b) we have

$$\frac{\partial \mathcal{V}}{\partial x} = \frac{V_B - V_A}{h_b + h_a} \quad (7) \quad \text{and} \quad \frac{\partial \mathcal{V}}{\partial y} = \frac{V_C - V_D}{h_c + h_d} \quad (8)$$

Applying Gauss' theorem for a closed surface of an arbitrary shape containing the hot conductor of  $s$  straight line segments each containing  $l$ , the charge per unit length normal to the cross section would then be given by

$$Q = \varepsilon_r \varepsilon_0 l \sum_s \sum_{p=1}^4 \left( \frac{\partial \mathcal{V}}{\partial n} \right)_p \quad (9)$$

where the apostrophe sign is used to indicate that the first and last terms in the summation are halved, that is seen to be equivalent to integration by the trapezoidal rule,  $l$  is the length of the infinitesimal segment of the integration path. For uniform discretisation,  $l$  is essentially the grid size  $h$ . For non-uniform grids,  $l$  is assumed to be either  $(h_a+h_b)/2$  or  $(h_c+h_d)/2$  depending on either a horizontal or vertical line segment over which the summation is taken. The relative permittivity,  $\varepsilon_r$  depends on the dielectric medium on which the point  $P$  is located. For example, a summation of the derivative along the first horizontal segment ( $s=1$ ) where it lies completely in the air, then  $\varepsilon_r=1.0$ . Similarly for segment 3 which is in the  $\text{LiNbO}_3$  crystal and  $\varepsilon_r = \varepsilon_z=43$ . For points which are entirely in the air,  $\text{SiO}_2$  and  $\text{LiNbO}_3$ , the relative permittivities are  $\varepsilon_a = 1.0$ ,  $\varepsilon_b=3.9$  and  $\varepsilon_x=28$ , respectively. However, for points on the buffer air interface, it can be assumed that half of the flux passes through each medium. So for air- $\text{SiO}_2$  interface,  $\varepsilon_r=(1+\varepsilon_b)/2$ . Whereas for the  $\text{SiO}_2$ - $\text{LiNbO}_3$  interface,  $\varepsilon_r=(\varepsilon_b+\varepsilon_x)/2$ . Using the charge capacity given by  $C = Q/V_t$  with  $V_t$  the potential difference between the conductors assumed be unity to simply our calculation,  $C_0$ , is obtained by solving the Laplace Equation for the transmission line in the air filled medium without the dielectric and similarly for estimating the charge capacity and thus the electrode capacitance. Once  $C_0$  and  $C$  are determined, both the characteristic impedance,  $Z$  and

microwave effective index,  $n_m$  can be determined by using (4) and (5).

### 2.3 Electro-optic modulation overlap integral and small signal frequency response

The electric fields of the travelling waves in the x and y directions can be determined from the electric potentials at grid locations as

$$E_x = \frac{\partial \mathcal{V}}{\partial x} = \frac{V_B - V_A}{(h_a + h_b)} \quad (10) \quad \text{and} \quad E_y = \frac{\partial \mathcal{V}}{\partial y} = \frac{V_c - V_D}{(h_c + h_d)} \quad (11)$$

The electro-optic interaction of the MZI modulator can thus be determined by the overlap integral,  $\Gamma$  which is given by <sup>[15,16]</sup>

$$\Gamma = \frac{g}{V} \iint |E_o(x, y)|^2 E_m(x, y) dx dy \quad (12)$$

where  $|E_o(x, y)|^2$  is the optical field intensity distribution of the optical guided waves and  $E_m$  is the electrical field of the electrodes. The choice of  $E_x$  or  $E_y$  depends on the crystal orientation and the polarisation of the optical field. We can indeed assume that the normalised optical field intensity profile assumes a Hermitian-Gaussian profile that is defined as <sup>[15,16]</sup>

$$|E_o(x, y)|^2 = \frac{4y^2}{w_x w_y^3 \pi} \exp\left[-\left(\frac{x-p}{w_x}\right)^2\right] \cdot \exp\left[-\left(\frac{y}{w_y}\right)^2\right] \quad (13)$$

where the  $1/e$  intensity width and depth are  $2w_x$  and  $1.376w_y$ , respectively, and  $p$  is the peak position of the optical field in the lateral direction.  $w_x$  and  $w_y$  are dependant on the fabrication parameters of the optical waveguide and can either be determined experimentally or by the optical waveguide mode modelling. We experimentally determine the optical fields by measuring these optical mode fields of optical waveguides fabricated by in-diffusion of the titanium strips into LiNbO<sub>3</sub>.

The small-signal bandwidth, i.e. in linear operating mode, is the most critical factor in the high frequency operation of the interferometric modulators. An applied RF voltage as seen at any point along the electrode by lightwaves that enter the waveguide at a time  $t_0$  can then be written as

$$V(z, t_0) = V_0 \sin\left[\frac{2\pi n_m f}{c} \left(1 - \frac{n_o}{n_m}\right) z - 2\pi f_0 t_0\right] \quad (14)$$

where  $n_o$  is the effective refractive index of the guided optical mode. For the interferometric modulators, the optical modulation is determined by the total induced phase shift introduced along the interaction length,  $L$ . The walk-off results in a frequency-dependent reduction in the integrated phase shift, which can be obtained by integrating the voltage that affects the light over the electrode length and given by

$$\frac{\int_0^L \Delta\beta(f) dz}{\Delta\beta} = \frac{\sin(\pi T f)}{\pi T f} \sin[\pi(2t_0 - T)f] \quad (15) \quad \text{with} \quad \overline{\Delta\beta} = \frac{\pi n_e r_{33} L V_0}{\lambda g} \Gamma \quad (16)$$

where  $n_e$  and  $r_{33}$  are the extraordinary index and electrooptic coefficient of LiNbO<sub>3</sub>, respectively,  $\lambda$  is the optical wavelength,  $g$  is the inter electrode gap, while  $T=L(n_m-n_o)/c$  is the transit time <sup>[30,31]</sup> resulting from the velocity mismatch between the co-propagating optical and microwave signals. For  $n_m=n_o$ , the optical wave travels down the waveguide at the same speed as the microwave drive signal travels along the electrode length, and consequently experiencing the same voltage over the entire electrode length. In this case the integrated value of  $\Delta\beta$  is proportional to  $V_0 L$ , and arbitrarily long electrodes can be used to reduce the required drive voltage with no frequency limitation. Unfortunately  $n_o \neq n_m$  so there is a walk off between the optical wave and microwave driven signal that results in a reduction of operation bandwidth, or, for sufficiently large length,  $L$  or frequency,  $f$ , a complete cancellation of  $\Delta\beta$ . In other words, in the design and implementation of electrodes, the microwave index,  $n_m$  must be as close as possible to the optical effective refractive index determined by the propagation of the guided lightwaves. This walk-off can be minimised by electroplating the electrode as thick as possible.

The frequency response of the interferometric modulators is given by the total phase shift resulted from an applied microwave voltage <sup>[4,30]</sup>

$$H(f) = e^{-(\alpha L/2)} \left[ \frac{\sinh^2\left(\frac{\alpha L}{2}\right) + \sin^2\left(\frac{\xi L}{2}\right)}{\left(\frac{\alpha L}{2}\right)^2 + \left(\frac{\xi L}{2}\right)^2} \right] \quad (17)$$

where  $\xi = 2\pi f(n_m - n_o)/c$  and  $\alpha$  is the attenuation constant due to electrical and dielectric loss which can be usually characterised by the measurement of the  $S_{12}$  scattering parameter of the microwave RF electrode. The 3 dB optical bandwidth is the electrical small signal 3 dB band under the condition that the modulators are biased in the linear region or at phase quadrature region where the optical output intensity is approximately a linear function of the applied voltage<sup>[30]</sup>, with  $V_\pi$  the DC bias voltage required to generate a phase difference  $\Delta\beta$  of  $\pi$  by  $V_\pi = \frac{\lambda g}{n_e^3 r_{33} L \Gamma}$ .

The overlap integral,  $\Gamma$ , can be calculated independently without affecting the impedance  $Z$  and effective microwave index  $n_m$  in the electrode design. In order to obtain a low  $V_\pi$ , the overlap integral is to be maximised that can be achieved by fabrication of Ti:LiNbO<sub>3</sub> (Titanium diffused lithium niobate) waveguide which could support tightest confined optical fundamental TE or TM mode. The bandwidth is determined as the 3-dB optical intensity modulation depth.

For systems where the originating and received signals are ultimately electrical, the electrical bandwidth is more relevant. The small signal bandwidth can be determined by solving (17) for the frequency at which  $H(f) = 1/\sqrt{2}$ . This can be found by using the bisection search algorithm. For a loss less electrode,  $H(f)$  is reduced to  $\text{sinc}(\xi L/2\pi)$  and the bandwidth would be approximated by

$$B.W \cong 1.4c / [\pi L(n_m - n_o)] \quad (18)$$

This expression can also be used as a rule of thumb for electrode design and allows us to calculate the required electrode length by specifying the optical bandwidth of the transfer function  $H(f)$  and how the difference in optical and microwave index,  $\Delta n = n_m - n_o$ , the loss constant,  $\alpha_0$  and the electrode length,  $L$  can affect the 3 dB bandwidth of the optical response. This 3 dB bandwidth of the modulator can thus be maximised by optimising  $\Delta n$  to its possible minimum value. These parameters can be optimised in the later section electrode losses, the bandwidth of travelling wave devices depends on the length, velocity mismatch and also the device type, which for our case is an interferometric type device.

### 3 DESIGN MODELLING AND IMPLEMENTATION

#### 3.1 Electrode structures and performance

Contour plots of the potentials, hence the electric fields for modulating the optical phase, for coplanar waveguide (CPW), asymmetric co-planar strip (ACPS) and co-planar strip (CPS) electrode structures can be obtained via the solutions of the above-described Laplace equations. These electrode structures are distinguished by whether one of the electrodes is used as an earth (for ACPS) or as both hot electrodes with an additional earth plane. Devices with dimensions  $w=10 \mu\text{m}$ ,  $g=15 \mu\text{m}$ ,  $t=3 \mu\text{m}$  and  $t_b=1.2 \mu\text{m}$  are used as an example. Once the electric fields  $E_x$ , and  $E_y$  of the travelling wave electrodes are obtained for each structure, the optical fields profile of the fundamental lightwave mode are designed for matching, hence broadband operations of the interferometric optical modulators.  $E_x$  component is strongest in region in the electrode gaps while  $E_y$  is strongest along the hot electrode region for all travelling type structures. We note also that the push pull operation can be achieved most efficiently by  $E_x$  of a co-planar waveguide electrode structure for the X-cut Y-propagating device.

Another structure consisting of optical waveguides positioned directly underneath is the CPS electrode by taking full and effective strength of  $E_y$  in a Z-cut LiNbO<sub>3</sub>. The CPS structure, however, suffers high propagation loss<sup>[20]</sup> and is therefore seldom used. Another common configuration for Z-cut device is to place one waveguide under the hot electrodes and the other at the edge of the ground plane in either the CPW or ACPS structure similar to the electrode incorporated in Figure 1.  $E_y$  is used in such configuration. This however cannot be considered as a full push-pull operation because the waveguide underneath the electrode ground plane effectively sees only half of the optical guided placed under the hot electrode. Strongest field exists around the edges of the electrodes, within the SiO<sub>2</sub> buffer layer underneath the hot electrodes and also in the gap between the electrodes. It is therefore necessary to assign denser finite difference grids in these regions.

In preliminary simulation a grid size as small as  $0.05 \mu\text{m}$  to  $0.2 \mu\text{m}$  at around the electrode edges is used, the gap and buffer region, up to larger grid size of  $8$  to  $10 \mu\text{m}$  for points where the electric field has decayed substantially and accurate results can be obtained. It is found that a problem space of around  $400$  by  $400 \mu\text{m}$  is sufficient to assume a 'metal box' boundary condition. An average grid size for that problem space would be about  $300 \times 200$  points. With the band storage mode employed by the matrix solver and a work-station environment, such dense grid mesh can be supported without difficulty. The average amount of time taken to complete a typical simulation would be around  $3$  to  $5$  minutes on a PC Pentium IV workstation. With this consumption of computing time current PCs with CPU clock rate of  $1.9 \text{ Gb/s}$  and  $512 \text{ Mbytes}$  RAM can be used to model these electrodes and optical modulation at ease.

### 3.1.1 Electrode modelling accuracy and comparisons with other techniques

We compare the values of  $Z$  and  $n_m$  with several published experimental results as tabulated in Table 1. The calculation of FDTWEA for both the CPW electrodes compares well with the measured results in Ref.[5].  $Z$  and  $n_m$  take values of  $0.6$  to  $0.85$  because these two values of  $t_b$  are determined from the tolerances of fabricated devices. Calculated results have agreed very well with measured values of fabricated modulators.

Ref.	Electrode	W( $\mu\text{m}$ )	g( $\mu\text{m}$ )	t( $\mu\text{m}$ )	$t_b$ ( $\mu\text{m}$ )	Published		FDTWEA	
						$n_m$	Z( $\Omega$ )	$n_m$	Z( $\Omega$ )
[5]	CPW	20	5	3	0.6-0.85	0.27	27	2.867 - 2.703	25.7- 27.3
	CPW	48	10	3	0.6-0.85	0.3	24.5	3.358 - 3.224	24.13 - 25.14
[22]	ACPS	15	5	4	0	-	~35	3.661	29.83
		15	5	0	0	-	-	4.226	35.315
[16]	ACPS	10	10	1.5	0.1	-	45(Cal) ,47.1(TDR) 49.8(NA)	3.781	45.27

**Table 1: FDTWEA calculated results as compared with published results**

There seems to be a discrepancy in our calculated  $Z$  value of the ACPS structure compared to that reported in Ref.[22]. However Ref.[22] has not indicated how the value  $Z$  of  $35 \text{ ohms}$  could be obtained. We therefore assume that in their calculations the thickness of the electrodes was not taken into account. We confirm this value by a calculation of the impedance in which an infinitely thin electrode is assumed and an impedance of  $35.315 \Omega$  is obtained. Our modelling is thus again confirmed with experimental results reported by Ref.[16] and is consistent with calculated results based on the method of image. However, the measured result differs slightly from the theoretical predictions as described above. The characteristic impedance measured by the time domain reflection and by using network analysis techniques was  $49.8 \Omega$  and  $47.1 \Omega$ , respectively. A slight discrepancy is possibly due to the effect of a thick  $\text{SiO}_2$  buffer layer.

The effective microwave index  $n_m$  for very thick electrodes agrees well with those obtained by the finite element method<sup>[13]</sup> and are shown in Figure 4. The thickness of the electrodes can significantly improve the electrical and optical velocity matching. Thick electrodes that are in the range of  $10$ - $20 \mu\text{m}$  are employed. Calculated results using finite difference approach and those by the finite difference method agree to within  $0.5\%$ . A grid size of  $0.125 \mu\text{m}$  along the wall of the thick electrodes is employed in our calculations. The finite difference scheme presented herein has achieved similar level of accuracy with highly efficient use of computing resources. Thus it can be employed for much more complex electrode structures in optical modulation systems such as a composite, cascaded or cascode electrode structures. It can be shown that the finite difference scheme is capable of calculating the travelling wave electrode parameters, namely  $Z$  and  $n_m$  with high precision. The FDTWEA is therefore an efficient package for the design of the design of travelling wave electrodes for integrated electro-optic interferometric intensity and other integrated phase modulators.

### 3.2 Electro-optic overlap integral factors

In this section, simulated results for the overlap integral between the travelling wave field and the optical guide waves are given. In order to compute the overlap integral, we need the normalised optical intensity field

profile that follows a Hermitian-Gaussian profile as given by (4). The mode size of the optical field influences the overlap integral  $\Gamma$ , and hence the modulation efficiency of the optical modulator. The variables that characterise the optical guided mode size are  $w_x$  and  $w_y$ , which are twice the 1/e modal width and 1.376 times the 1/e modal depth.  $w_x$  and  $w_y$  can either be calculated using standard modelling of optical fields in channel optical waveguides or by experimentally measured mode size. Another important attribute is that affects  $\Gamma$  is the relative position of the optical mode with respect to the hot electrodes. All the attributes that affect the value of  $\Gamma$  can be easily modelled by FDTWEA.  $\Gamma$  for the ACPS electrodes and effects of various factors on this overlap integral are given. The ACPS is most preferred in a double modulator structure for carrier suppressed return-to-zero (CS-RZ) intensity modulators in OC-768 40 Gb/s optical fibre communications systems due to its simplicity in launching the RF travelling waves into one electrode rather than that in the CPS where two in-phase microwaves must be excited and the control of the electrical phase in these two electrodes is much more difficult.

Figure 5(a) shows the variations of the overlap integral,  $\Gamma$  as the peak position of the optical mode,  $\pi$  shifts from one end of the electrodes to the other end. The plots indicate quantitatively how the spot size of the optical mode field influence the overlap integral factor  $\Gamma$ . As expected, a tighter confined mode would give a higher value of  $\Gamma$ . It is therefore important to design and fabricate Ti-diffused LiNbO<sub>3</sub> waveguide that can give the smallest possible mode size. Apart from having a tightly confined optical mode, the relative position of the optical waveguide with respect to the electrodes is also extremely important to maximise the contribution of the electro-optic effect. When narrow electrodes are used with the electrode width comparable to the size of the waveguide, then it is preferred to place the waveguide directly underneath the electrode to utilise the strong edge field from both side of the electrode. This has been shown in Figure 5(b) where maximum  $\Gamma$  is obtained when the position of an optical waveguide of the interferometer is centred under the electrode. However, for a much wider electrode width, the preferred position would be just inside the end of the electrode closer to the gap when a 30 $\mu$ m wide electrode is employed. A maximum overlap integral can be achieved by exploiting the higher edge field by centralising the waveguide at  $x \sim 135 \mu$ m.

### 3.3 Effects of angled-wall structure on RF electrodes

In previous sections, FDTWEA has been used to analyse various rudimentary design parameters of the travelling wave electrodes. This technique has been employed to accurately analyse non-ideal electrode structures such as shielded phase velocity-matching travelling wave electrode structure proposed by Kawano et al.<sup>[11-12]</sup>. Further the analysis of wall-angled electrodes as proposed by Gopal et al.<sup>[21]</sup> is also analysed and confirmed by our method. Again in this section the FDTWEA is used to investigate the effect of the electrode wall angle that exhibits in the fabrication of thick electrode by electro-plating. In extending the bandwidth of the device, very thick electrodes of thickness ranges from 10-20  $\mu$ m is used. Such fabricated thick electrodes, however, do not assume a perfect 'brick wall' shape. Such geometrical factor cannot be ignored because they certainly have a subtle effect on both the values of  $Z$  and  $n_m$ . Gopal et al.<sup>[21]</sup> have modelled the effect with their finite element calculation. We shall examine the effects of the wall angle using the above described finite difference model to demonstrate the capability of our numerical model. Similar electrode structures and dimensions similar to that reported in Ref.[21] have been adopted in our experimental works.

The wall-angle of the tilted electrodes significantly affects the effective values of  $Z$  and  $n_m$  as shown in Figure 6. The effect of the wall angle is less severe for thinner electrodes. For thick electrodes, especially those that are greater than 10  $\mu$ m, the wall angle effect must not be ignored. For example, if we base our design on the assumption of a  $\theta=90^\circ$  rectangular electrode, then we would use a 20  $\mu$ m thick electrode for the best velocity match. However if the fabricated electrodes actually assume a trapezoidal shape with  $\theta=80^\circ$ , we would have overestimated the value of  $n_m$  for best velocity matching by about 0.2. This corresponds to almost a 20% error in the estimation of the MZI modulator bandwidth. Calculated and experimental results indicate that an electrode thickness of around 14 $\mu$ m can be used to achieve maximum bandwidth. Based on the assumption of an 82 $^\circ$  electrode wall angle and an electrode of a thickness of 15  $\mu$ m<sup>[21]</sup>. We have thus shown another potential application of our developed finite difference numerical modelling scheme with accuracy higher than that would be beyond most analytical techniques such as the Green function method<sup>[4,5]</sup>, the spectral domain analysis<sup>[9]</sup>, conformal mapping<sup>[1]</sup>, or method of image<sup>[3,15]</sup>.

### 3.4 MZI modulator implementation

Optical waveguides are fabricated by Ti:diffusion of about 500  $\text{Å}$  thick under a diffusion time of 7 hours. SiO<sub>2</sub> layer is then sputtered with thickness variable from 0.6 to 2.0  $\mu$ m. Electrodes are formed by two main stages. A 200  $\text{Å}$  chrome layer is first deposited and the electrode pattern is then photolithographic ally created. A 1000  $\text{Å}$  thick Au layer is then deposited on the Cr patterned electrode. The gold layer is then etched to the pattern of the electrode structures. Electroplating of thick Au pattern is then conducted. The thickness of electroplated

Au can reach 7 to 10  $\mu\text{m}$  with a wall angle of about 12 to 20 degrees without shorting the electrodes. Note that prior to the fabrication of the electrode, optical channel waveguides are tested using the straight optical channels pattern next to the Mach-Zehnder structures in order to determine the important parameters of the electrodes as designed and simulated. Microwave coupling and mounting are packaged and fibre pigtailed are then performed.

The insertion loss  $S_{21}$  of the fabricated electrodes are simulated and measured and are consistent as predicted and shown in Figure 7. Figure 8 shows the measured RF insertions loss with the upper curve showing the calibrated  $S_{21}$  of the microwave set up and the lower curve showing the results for the case when the RF electrodes are included in the measured system. Several modulators have been fabricated. The obtained results indicate that the electrical and optical bandwidths reach a consistent range of about 26 GHz to 30 GHz. Optical measurement of the packaged modulators have also been obtained and the optical transfer bandwidths are compatible with those obtained in the electrical domain. It can be concluded that the optical loss is minimum and a good velocity matching between the optical waves and the travelling microwaves. Experimental results will be described in details. Further experimental results of several broadband modulators would be presented.

#### 4 CONCLUSION

A numerical model has been modulated to conduct analytical, effective and efficient modelling of electrode performance and electro-optic interaction for optical modulation of guided lightwaves via the interferometric structures. The anisotropic Laplace equation (1) can be used and solved using the finite difference techniques that lead to an accurate and efficient model of the microwave properties of various electrode structures. A non-uniform grid allocation scheme is employed to reduce the size of computing memory. The numerical FDTWEA has been shown to be efficient without jeopardising the accuracy. Calculated values of the characteristic impedance  $Z$  and the microwave effective index  $n_m$  obtained by this method are consistent with those reported in published articles. Comparison of FDTWEA' calculations with the finite element method<sup>[19, 20]</sup> has promised consistency of the two computation techniques and hence the effectiveness of the finite difference presented in this paper, in computing resources and potentials in its applications in complex electrode structures of optical modulators.

The FDTWEA has been incorporated in interferometric modulators in estimating the interaction overlap integral,  $\Gamma$  allowing the design of a low half wave voltage,  $V_{\pi} \cdot \text{Hev}\chi\epsilon$  lower power driven optical modulator can be realised. It is shown that FDTWEA can be used effectively in analysing the electrode of practical modulators. The effects of the trapezoidal shape electrode with the wall angle  $\theta$  are described which could not be easily modelled by most analytical techniques such as the conformal mapping method of image, Green function method or spectral domain analysis.

Experimental results have been obtained for optical MZ modulators with an electrical/optical bandwidth reaching 26 to 30 GHz with an electrode thickness of more than 5  $\mu\text{m}$  and an estimate wall angle of about 12 degrees. This indicates the accuracy of the electrode modelling and the simple fabrication techniques of the electrodes and optical waveguide structures.

#### REFERENCES

1. O.G.Ramer, IEEE J. Quant. Elect., **QE-18**, pp.386-392, 1982.
2. D. Marcuse, IEEE J. Quant. Elect., **QE-18**, pp.393-398, 1982.
3. C. Sabatier and E. Caquot, IEEE J. Quant. Elect., **QE-22**, pp. 32-37, 1986
4. H.Chung, W.S.C. Chang, and E.L. Adler, IEEE J. Quant. Electron., **QE-27**, pp.608-617, 1991.
5. H. Chung, W.S.C. Chang, and G.E. Betts, IEEE J. Lightw. Tech., **11**, pp.1274-1278, 1993.
6. M. Seino, et al, Proc. ECOC '90, pp.999-1002, postdeadline paper, 1990.
7. R.A. Becker, "Broadband guided wave electrooptic modulators", IEEE J. Quant. Elect., **QE-20**, pp.723-727, 1984.
8. H. Jin, M. Bélanger and Z. Jakubezyk, IEEE J. Quant. Elect., **27**, pp.243-251, 1991.
9. K. Kawano et al., IEEE Photonics Tech. Lett., **1**, pp. 33-34, 1989.
10. T. Kitoh and K. Kawano, Elect. & Comm. Japan, Part 2, **76**, pp.25-34, 1993.
11. K. Kawano et al., Elect. Lett., **25**, pp. 20-21, 1989.
12. K. Kawano et al., Elect. & Comm.Japan, Part 2, **75**, pp. 9-19, 1992.
13. see for example (a) Z. Pantic and R. Mittra, IEEE Trans. Microw. Th. Tech., vol. MTT-34, no. 11, Nov. 1986 and (b) M. Hoshiba, T. Tsuji and M. Nisho, IEEE Trans. Microw. Th. Tech., **47**, pp. 1627-1633, 1999.
14. K. Kenji, N. Kazuto, T. Kitoh and H. Miyazawa, IEEE Photonics Tech. Lett., **3**, 1991.
15. W-C. Chuang et al., J. Opt. Comm, **14**, pp. 142-148, 1993.
16. C.M Kim and R. Ramaswamy, IEEE J. Lightwave Tech., **7**, pp.1063-1070, 1989.
17. E.L. Wooten and W.S.C. Chiang, IEEE J. Quant. Elect., **29**, pp.161-170, 1993.
18. N.H. Zhu, Z.Q. Wang, Opt. Quant. Elect. **27**, pp.607-615, 1995.
19. H.E. Green, IEEE Trans. Microw. Th. Tech., **MTT-13**, pp.676-692, 1965.
20. G.K. Gopalakrishnan et al., Elect. Lett., **28**, pp. 207-208, 1992.
21. G.K. Gopalakrishnan et al., IEEE J. Lightw. Tech., **12**, pp. 1807-1818, 1994.
22. S.K. Korotky et al., App. Phys. Lett., **50**, pp.1631-1633, 1987.
23. C.M Gee et al., App. Phys. Lett., **43**, no. 11, 1 Dec. 1983.
24. W. Charczenko et al., IEEE J. Lightwave Tech., **9**, pp.92-100, 1991.

25. S.Y. Liao, Microwave Circuit Analysis and Amplifier Design, Prentice-Hall Int. Ed..
26. K. Atsuki and E. Yamashita, IEEE J. Lighwave Tech., **LT-5**, pp. 316-319, 1987.
27. S. Ramo and R.W. Whinery, "Fields and Waves in Communication Electronics", 2<sup>nd</sup> Ed., J. Wiley.
28. D. Hoffman, Fortran 77: A Structured, Discipline Style, 2<sup>nd</sup> Ed., McGraw Hill Book Co.
29. M. R. Spiegel, Mathematical Handbook of Formulas and Tables, Shaum's Outline Series, McGraw hill Book Co.
30. W. H. Press et al., Numerical recipes-the art of scientific computing, Cambridge Univ. Press, pp.240-246.
31. T. C. Oppe et al., NSPCG user's guide V. 1.0 - a package for solving large sparse linear systems by various iterative methods, Center for Numerical Analysis, University of Texas, Austin., USA
32. T. Tamir, Guided-Wave Optoelectronics, 2<sup>nd</sup> Ed., Springer-Verlag.
33. R. Kraehenbuehl and W.K. Burns, IEEE Trans. Microw. Th. Tech., **48**, pp.860-864, 2000.

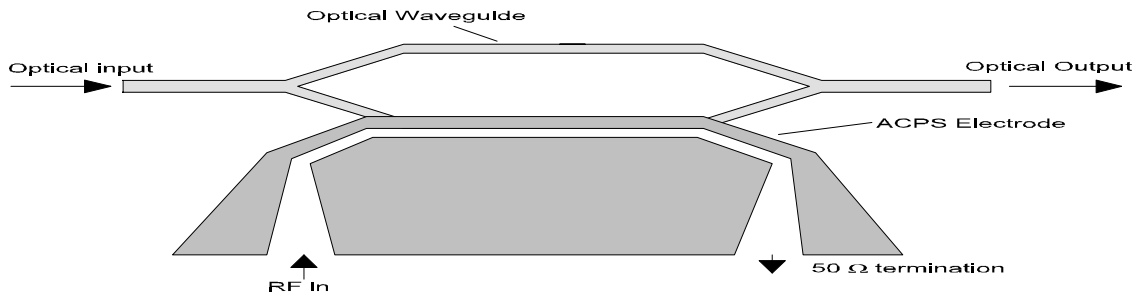


Figure 1(a)

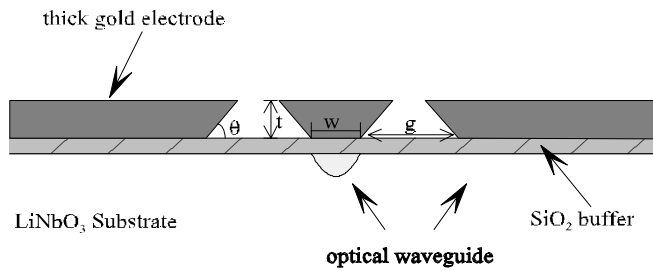


Figure 1(b)

Figure 1 (a) Schematic diagram of the electro-optic interferometric modulator (b) cross sectional view of wall-angle tilted thick electrodes deposited and plated above the diffused integrated optical waveguides.

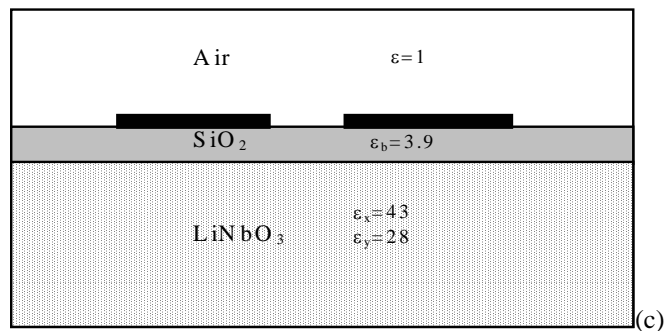
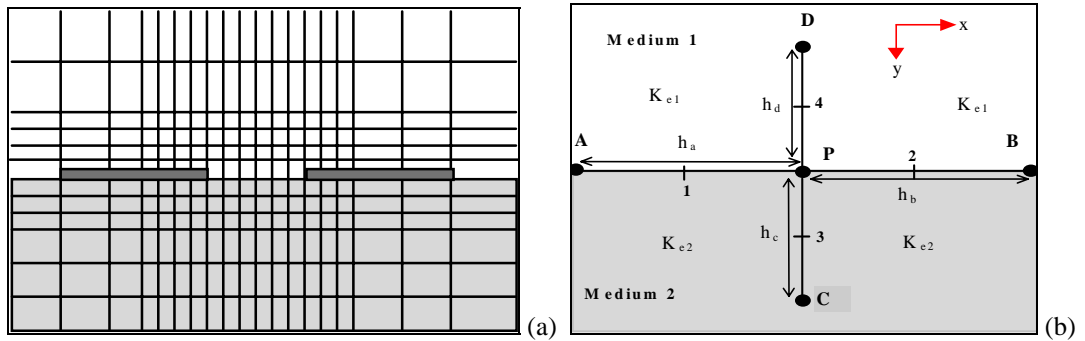


Figure 2 Development of the geometrical topology for finite difference modeling for integrated optical modulator (a) the non-uniform grid allocation scheme and (b) the grid points for finite differencing and (c) the dielectric boundaries

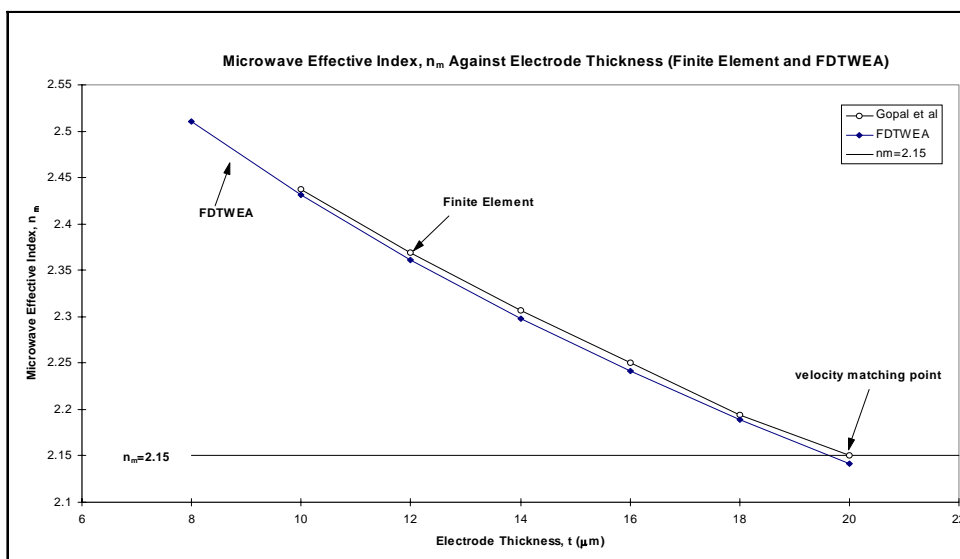


Figure 4  $n_m$  calculated by FDTWEA and compared with those obtained by the finite element method

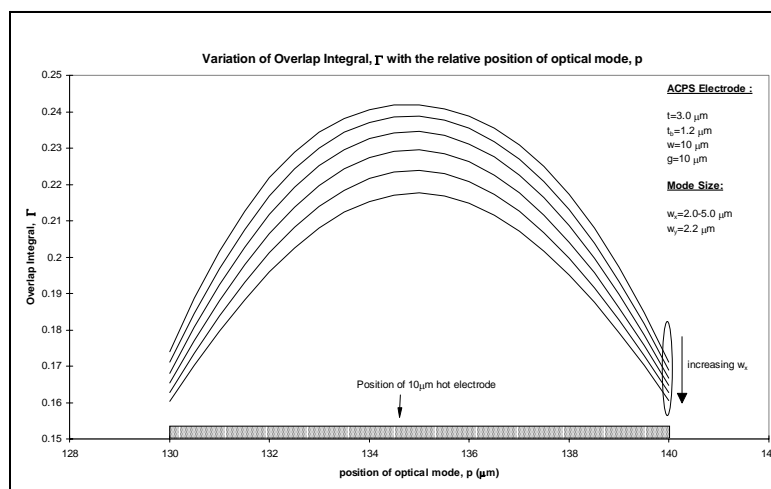


Figure 5(a)

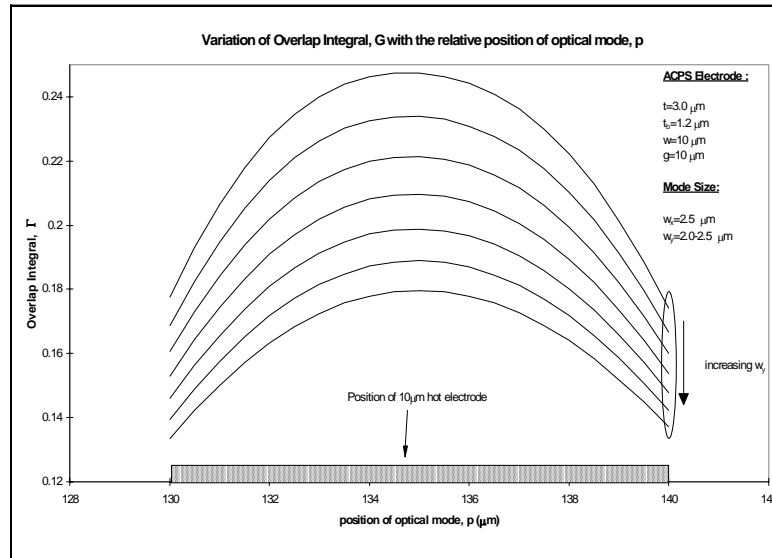


Figure 5(b)

Figure 5 Variation of the overlap integral  $\Gamma$  with the peak position of the optical mode shifting from one end of the hot electrode to the other (a) for widening the optical guided mode (b) for increasingly deeper optical mode

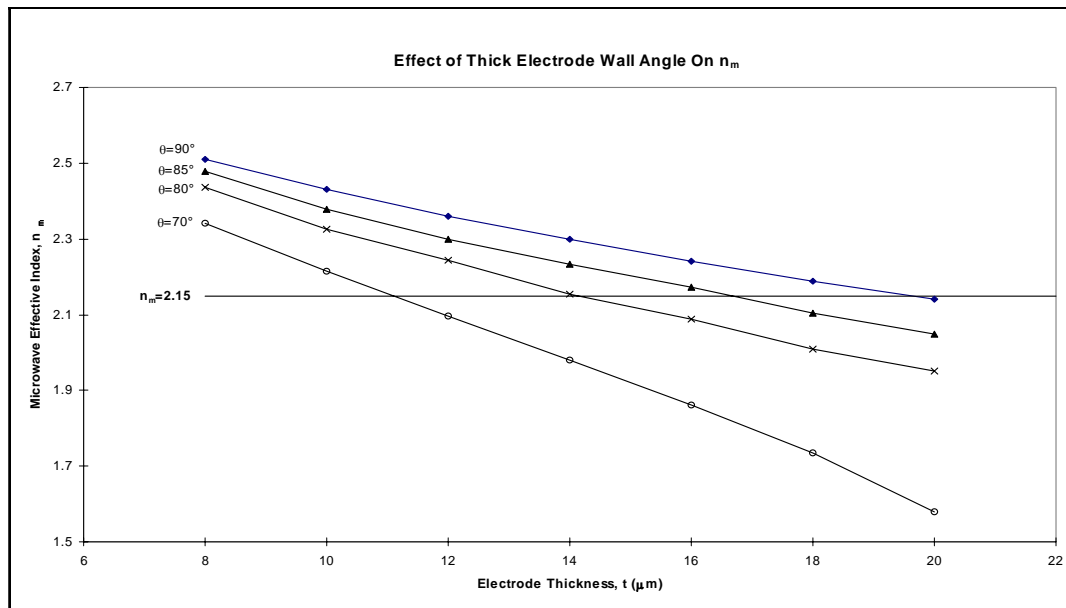


Figure 6 Dependence on  $n_m$  and  $Z$  on the wall angle of the thick gold plated electrode.

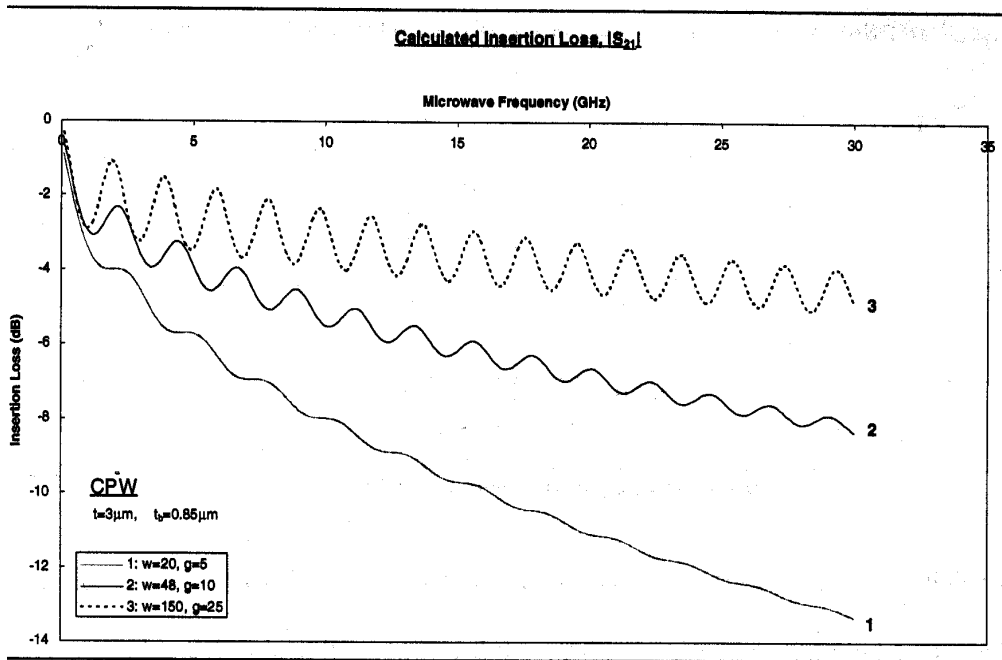


Figure 7 Insertion loss  $S_{21}$  of the RF electrode as a function of the microwave frequency

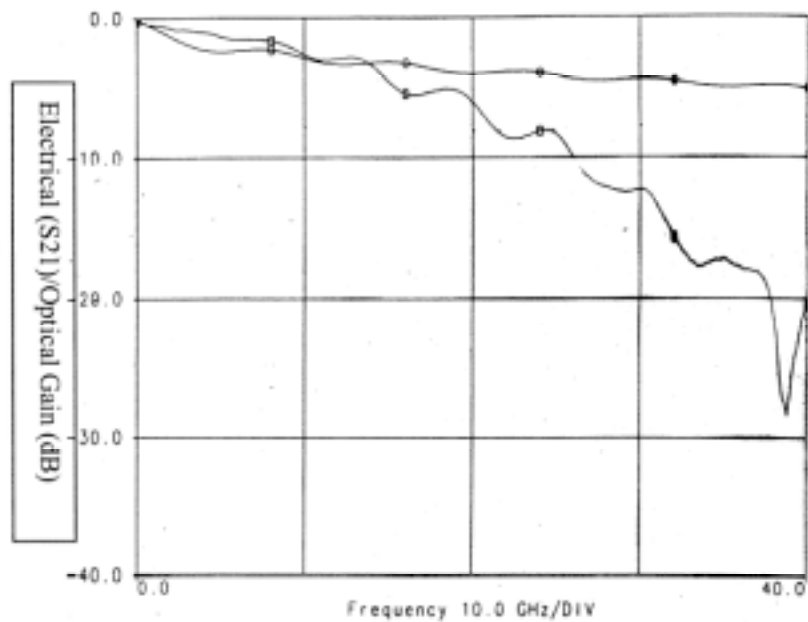


Figure 8 Electrical ( $S_{21}$ )/Optical response of a fabricated interferometric modulator. Upper curve shows response of measurement set up and the other the optical "gain" output response.